Charge-Carrier Mobility Requirements for Bulk Heterojunction Solar Cells with High Fill Factor and External Quantum Efficiency >90%

*Jonathan A. Bartelt, David Lam, Timothy M. Burke, Sean M. Sweetnam, and Michael D. McGehee**

Dedicated to Frank on the occasion of his 15th birthday

To increase the efficiency of bulk heterojunction (BHJ) solar cells beyond 15%, 300 nm thick devices with 0.8 fill factor (FF) and external quantum efficiency (EQE) >90% are likely needed. This work demonstrates that numerical device simulators are a powerful tool for investigating charge-carrier transport in BHJ devices and are useful for rapidly determining what semiconductor properties are needed to reach these performance milestones. The electron and hole mobility in a BHJ must be ≈10^{-2} cm^2 V^{-1} s^{-1} in order to attain a 0.8 FF in a 300 nm thick device with the recombination rate constant of poly(3-hexylthiophene):[6,6]-phenyl-C61-butyric acid methyl ester (P3HT:PCBM). Thus, the hole mobility of donor polymers needs to increase from ≈10^{-4} to ≈10^{-2} cm^2 V^{-1} s^{-1} in order to significantly improve device performance. Furthermore, the charge-carrier mobility required for high FF is directly proportional to the BHJ recombination rate constant, which demonstrates that decreasing the recombination rate constant could dramatically improve the efficiency of optically thick devices. These findings suggest that researchers should prioritize improving charge-carrier mobility when synthesizing new materials for BHJ solar cells and highlight that they should aim to understand what factors affect the recombination rate constant in these devices.

1. Introduction

The external quantum efficiency (EQE) and fill factor (FF) of single-junction bulk heterojunction (BHJ) solar cells likely need to approach 90% and 0.8, respectively, in order for these devices to reach 15% power conversion efficiency (PCE).[1–6] BHJ solar cells with FF ≈0.8 have already been reported,[3,7] which demonstrates that these devices are able to match the high FFs attained by inorganic devices.[8] Achieving a 90% EQE while maintaining a high FF, however, has proved difficult with BHJ devices.

The active layer in a solar cell must absorb at least 90% of the incident photons with above bandgap energy in order to achieve an EQE ≥90%. A typical BHJ device with a metal back reflector reaches 90% absorption when the active layer is >200 nm thick, while a semitransparent device (such as a subcell in a tandem solar cell) requires a >300 nm thick active layer to absorb the same amount of light. Several BHJ materials systems have achieved internal quantum efficiency (IQE) ≥90%,[5,9–11] but these devices were optimized with ≈100 nm thick active layers and the device EQE was ≤80% due to insufficient absorption. When these devices were made thicker to improve light absorption, the FF decreased, leading to an overall decline in solar cell PCE.[11–13] Increasing the active layer thickness in a BHJ solar cell often degrades device performance because charge carriers must travel farther through a thick active layer in order to reach the device electrodes. Furthermore, the magnitude of the built-in electric field across the device decreases when the active layer is made thicker. Both of these factors increase the time needed to extract the charge carriers generated in a device, which increases the probability that the charge carriers will recombine before they are extracted from the device.

Space-charge buildup also contributes to poor device performance in optically thick BHJ solar cells. In devices with low or imbalanced charge-carrier mobility, the charge carriers with the lowest mobility can build up in the active layer, which creates space-charge and screens the built-in electric field across the device.[11–19] Several polymers with relatively high hole mobility (>10^{-3} cm^2 V^{-1} s^{-1}) have recently achieved FF >0.7 in devices with active layers >300 nm thick.[3,6,7,18] These results suggest

J. A. Bartelt, T. M. Burke, Dr. S. M. Sweetnam, Prof. M. D. McGehee
Department of Materials Science and Engineering
Stanford University
Stanford, CA 94305, USA
E-mail: mmcgehee@stanford.edu

D. Lam
Department of Physics
Stanford University
Stanford, CA 94305, USA

DOI: 10.1002/aenm.201500577

that higher polymer hole mobilities are needed to prevent space-charge buildup and limit recombination in optically thick BHJ devices. How high the charge-carrier mobilities need to be in order to achieve FF ≈0.80 in an optically thick device, however, has not yet been determined.

In this report, we demonstrate that numerical 1D drift-diffusion device simulators, which are routinely used by inorganic solar cell researchers[20–22] but used to a lesser extent by organic solar cell researchers,[23–26] are a powerful tool for investigating recombination and charge-carrier transport in BHJ solar cells. The morphology of polymer–fullerene BHJs is complex because these molecular mixtures are composed of two different semiconducting materials and consist of multiple phases of varying composition.[27–29] By using an effective medium approach to model the optical and electrical properties of BHJs, we are able to simulate the performance of these complex devices with relatively few fit parameters and experimentally measured inputs. Specifically, we use the device simulator to quantitatively determine the charge-carrier mobility required to achieve FF ≈0.8 in BHJ solar cells that are optically thick. Furthermore, we investigate the effects of the recombination rate constant on device performance and find that the charge-carrier mobility required for high FF is directly proportional to the recombination rate constant. Thus, reducing the recombination rate constant of BHJ solar cells would significantly reduce the charge-carrier mobility needed for high FF. To validate the device simulator, we fabricated a large variety of BHJ solar cells with hole mobility ranging from 1.6×10^{-7} to 3.6×10^{-4} cm^2 V^{-1} s^{-1} and active layer thickness ranging from 60 to 350 nm. We reproduced the wide range of experimental device results with the device simulator using only two fit parameters and the experimentally measured electron and hole mobility. Our results suggest that researchers should prioritize improving charge-carrier mobility when synthesizing the next generation of semiconducting materials for BHJ solar cells, and highlight that they should aim to understand what factors affect the recombination rate constant in these devices. Moreover, our findings show that device simulators provide valuable insights into BHJ solar cell operation and can be used to rapidly determine how certain variables affect device performance.

2. Results

2.1. Performance of Bulk Heterojunction Solar Cells

Mihailetchi et al.[30] demonstrated that one can tune the electron and hole mobility in poly(3-hexylthiophene):[6,6]-phenyl-C_{61}-butyric acid methyl ester (P3HT:PCBM) solar cells by thermally annealing the devices at temperatures ranging from 25 to 150 °C. For the purposes of validating the device simulator, we fabricated P3HT:PCBM devices with this procedure and annealed the devices at either 25, 48, 71, 88, 111, or 148 °C. The P3HT hole mobility in these devices was measured with hole-only diodes and a space-charge-limited current (SCLC) analysis, while the electron mobility was extrapolated from the work of Mihailetchi et al.[30] We find that annealing the P3HT:PCBM devices at 148 °C increases the hole mobility of P3HT by a factor of ≈2300, similar to the result reported by Mihailetchi et al. (an increase of ≈3300). In contrast, the electron mobility of PCBM is more stable and only increases by a factor of ≈30 after annealing at 148 °C. **Table 1** summarizes the hole and electron mobility in the P3HT:PCBM devices for the different anneal temperatures used in this study.

Table 1. Hole (μ_h) and electron (μ_e) mobility and photovoltaic performance of thermally annealed P3HT:PCBM BHJ solar cells.

Anneal temp. [°C]	μ_h [cm^2 V^{-1} s^{-1}]	μ_e [cm^2 V^{-1} s^{-1}]	Thickness [nm]	PCE [%]	FF	V_{OC} [V]	J_{SC} [mA cm^{-2}]
25	1.6×10^{-7}	1.5×10^{-4}	205	0.60	0.30	0.63	3.0
48	2.0×10^{-6}	2.5×10^{-4}	202	1.1	0.37	0.62	4.7
71	2.3×10^{-5}	1.0×10^{-3}	229	2.2	0.42	0.59	8.7
88	5.5×10^{-5}	1.5×10^{-3}	227	2.6	0.50	0.57	9.3
111	1.3×10^{-4}	3.0×10^{-3}	211	3.1	0.55	0.56	9.9
148	3.6×10^{-4}	5.0×10^{-3}	197	4.1	0.69	0.60	10.1

Note that the thickness data correspond to the solar cells and not the mobility data.

We fabricated solar cells with active layer thickness ranging from 60 to 350 nm for each anneal temperature. Table 1 shows the PCE, FF, V_{OC}, and short-circuit current (J_{SC}) for representative devices that are ≈200 nm thick, and **Figure 1**a shows the current density–voltage (J–V) curves for these devices. The 25 °C device performs poorly and has PCE <1% and a 0.30 FF. The PCE, FF, and J_{SC} of these devices increase significantly as the anneal temperature increases and the 148 °C device is optimized with 4.1% PCE and a 0.69 FF.

In this study, we focus on how the device FF changes with charge-carrier mobility and active layer thickness. As shown in **Figure 2**a, the 25 and 48 °C devices have low FF across all thicknesses tested. The FF of these devices increases modestly for the thinnest devices, but for active layers thicker than 100 nm the FF remains approximately constant at <0.4. In contrast, the 71, 88, and 111 °C devices have FFs that start at ≈0.68 for the thinnest devices and then gradually decrease to 0.37, 0.45, and 0.52, respectively, as the active layer thickness is increased. The 148 °C device displays another trend, which is a ≈0.7 FF that remains relatively constant across all active layer thicknesses tested. The strong correlation between charge-carrier mobility and FF suggests that altering charge-carrier mobilities has a significant effect on the performance of P3HT:PCBM solar cells.

2.2. Validation of the Numerical Device Simulator

To understand the trends in device performance in Figure 2, we used the Setfos 4.0 commercial device simulator (FLUXiM AG) which utilizes transfer matrix modeling to determine layer specific absorbance in a device and numerically solves the drift-diffusion equations to simulate the device J–V curve. Because the device simulator accounts for optical interference effects, we do not need to assume uniform light absorption throughout the active layer and can precisely determine the charge-carrier generation profile within the device. For our simulations, we used a device stack consisting of glass (500 nm), indium-doped tin oxide (115 nm), poly(3,4-ethylenedioxythiophene):poly(styrene

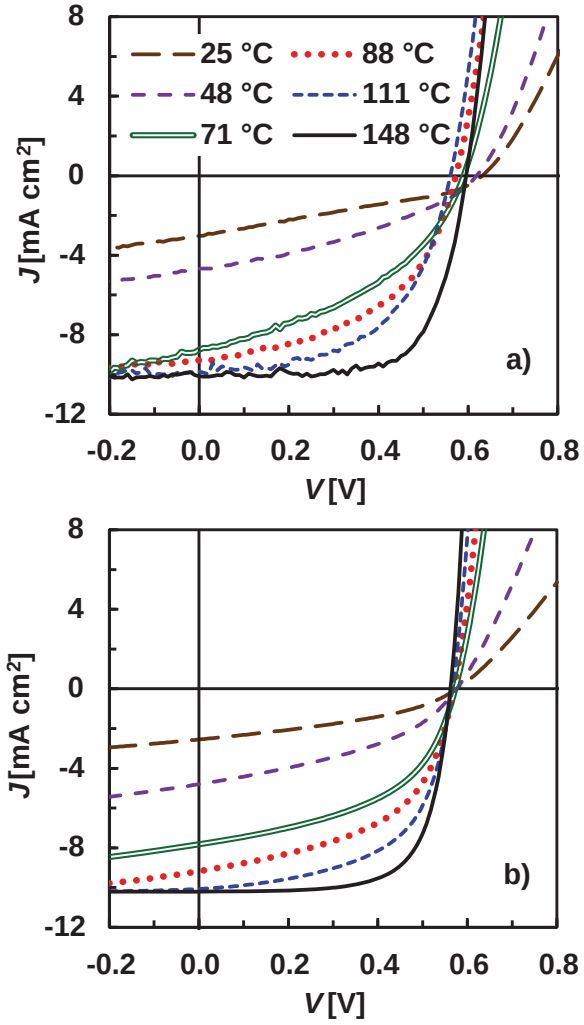

Figure 1. a) Experimentally measured and b) simulated current density–voltage (*J*–*V*) characteristics of thermally annealed ≈200 nm thick P3HT:PCBM BHJ solar cells. The anneal temperature is noted within the figure.

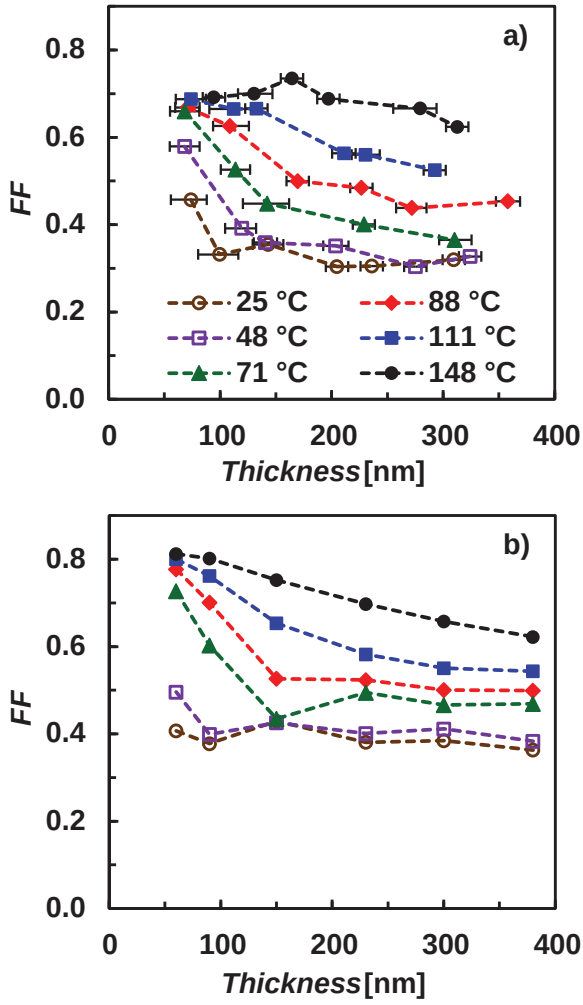

Figure 2. a) Experimentally measured and b) simulated fill factor versus active layer thickness for thermally annealed P3HT:PCBM solar cells. The thermal anneal temperature is noted within the figure.

sulfonate) (PEDOT:PSS) (35 nm), P3HT:PCBM (variable thickness), and aluminum (150 nm), which closely matches our experimental device. We assumed recombination in our devices is a bimolecular process and the rate of recombination, *R*, is described by the law of mass action (Equation (1)), where *k* is the recombination rate constant and *n* and *p* are the electron and hole density, respectively, in the solar cell.

$$R = knp \tag{1}$$

We only included bimolecular recombination in our model because recent experimental results have shown that the dominate recombination mechanism in high-performance BHJ solar cells is bimolecular recombination.[31–34] Additional recombination mechanisms may be needed to accurately model the performance of poorly performing devices, but the focus of this study is on simulating the performance of devices with high FF and EQE. We did not calculate the bimolecular recombination rate with the commonly used Langevin expression[23–25,35] because this expression assumes that every electron–hole encounter in the solar cell leads to recombination. Recent experiments[36,37] and simulations[38,39] have demonstrated that in high-performance BHJ solar cells the electron and hole are most likely to reseparate into free charge carriers after a given encounter, rather than recombine. Furthermore, we assumed that the geminate pair splitting efficiency in our simulations was not electric field-dependent and that absorbed photons directly generate free electrons and holes (i.e., no geminate recombination). This assumption is based on recent findings that show that the geminate pair splitting efficiency is independent of electrical bias in several high-performance BHJ solar cells.[31,36,38,40,41] For polymer–fullerene systems that do exhibit electric field-dependent geminate splitting, this assumption is not valid and geminate recombination should be incorporated into the simulations. We determined *k* for our P3HT:PCBM devices iteratively until a best fit was found between the experimental and simulated *J*–*V* curves (Figure S6, Supporting Information). We find $k \approx 2 \times 10^{-12}$ cm^3 s^{-1}, which agrees well with experimentally measured values of *k* for P3HT:PCBM solar cells.[31,42,43]

A detailed explanation of the assumptions and simulation parameters used for this study is included in the Experimental Section.

We simulated P3HT:PCBM solar cells that have been annealed at different temperatures using a constant value for k (2×10^{-12} cm^3 s^{-1}) and the appropriate SCLC charge-carrier mobilities from Table 1. Only two fit parameters, k and the series resistance (see the Experimental Section) were used to simulate a wide variety of experimental devices with FF varying from 0.3 to 0.7 and PCE varying from <0.5% to 4%. We find that the shape of the simulated J–V curves is in good agreement with the shape of the experimentally measured J–V curves (Figure 1b). Furthermore, the device simulator qualitatively reproduces the experimentally measured FF versus device thickness trends (Figure 2b). The simulator predicts that the FF of the 25 and 48 °C devices will be low and relatively constant across the device thicknesses tested and that the 71, 88, and 111 °C devices will transition from high FF to low FF as the device thickness is increased. To further validate the device simulator, we examined how the FF of P3HT:PCBM solar cells changes as a function of incident light intensity. The experimental and simulated trends in FF versus light intensity agree well, which provides further evidence that the simulator accurately models recombination in our devices (Figure S1, Supporting Information). We note that charge-carrier transport in BHJs is dispersive and modeling these devices with a single value of charge-carrier mobility does not account for the complex distribution of mobilities present in BHJs.[41,44] That said, the simulator is able to reproduce the experimental device performance quite well using single values for the electron and hole mobility, which shows that the effective medium approach and SCLC mobility values do indeed have merit. Furthermore, the SCLC mobility is relatively easy to measure and there are numerous SCLC mobilities reported in the literature, which makes this mobility metric valuable for material comparisons.

The device simulator predicts that the FF of the 71, 88, 111, and 148 °C devices should reach ≈0.8 for 60 nm thick devices, rather than ≈0.7 as observed in the experiment. The shunt resistance in the experimental devices decreases significantly for active layers <100 nm thick, so shunt pathways likely limit the FF of our thin experimental devices to ≈0.7 (Figure S2, Supporting Information). Other differences between the simulated and experimental results may be due to changes in BHJ morphology that occur when devices are thermally annealed. During thermal annealing, the P3HT degree of crystallinity increases[45,46] and the polymer–fullerene miscibility changes.[11,47,48] The formation of pure phases decreases the volume fraction of the BHJ that is molecularly mixed and reduces the number of donor–accepter heterojunctions where recombination occurs.[42,49] Furthermore, the energy levels in BHJs are sensitive to the polymer and fullerene morphology[50] and the charge-transfer state energy can be affected by thermal annealing.[51] Because we use the same value of k to simulate all the devices in Figures 1b and 2b, some elements of the changing morphology and energetics are not captured by our simulations. However, we believe the qualitative similarities between the experimental and simulated J–V curves show that the device simulator captures the essential physics that govern charge-carrier transport in BHJ solar cells.

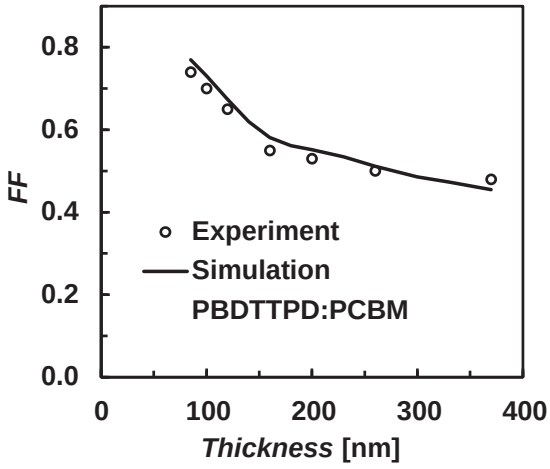

Figure 3. Experimentally measured and simulated fill factor versus active layer thickness for PBDTTPD:PCBM solar cells.

The device simulator also accurately models the performance of BHJ solar cells composed of the donor–acceptor copolymer, poly(di(2-ethylhexyloxy)benzo[1,2-*b*:4,5-*b*′]dithiophene-*co*-octylthieno[3,4-*c*]pyrrole-4,6-dione) (PBDTTPD), and PCBM (**Figure 3**). Devices made with PBDTTPD have achieved PCE as high as 8.5% with ≈100 nm thick active layers,[28,52] but suffer from poor FF when the devices are made thicker to improve absorption.[11] Using a constant value of k, we were able to accurately reproduce the experimental performance of PBDTTPD:PCBM BHJ solar cells with active layer thickness ranging from 85 to 370 nm (see the Experimental Section for details). This result further verifies that the device simulator accurately models charge-carrier transport in BHJ solar cells.

2.3. Space Charge Degrades Device Performance

Because the device simulator solves the continuity and Poisson equations at every location in the active layer, one can generate band diagrams for the simulated solar cells and gain insight that is not easily accessible via experiment. **Figure 4** shows the band diagram for 300 nm thick devices that have been annealed at 25 and 148 °C. For the 25 °C device, only ≈40 nm of active layer is under a significant electric field, even at J_{SC}. Across the majority of the active layers, the bands are flat and the electric field is screened by space charge. Because $\mu_e >> \mu_h$ in our P3HT devices, it takes longer to extract a hole from the device when compared to an electron traveling the same distance in the same electric field. The longer transit time for holes leads to the buildup of holes in the active layer, creating space charge. This space charge creates an electric field that screens the built-in field across the device and adversely affects charge transport in the device. This finding is in line with previous research showing that low hole mobility can lead to space-charge buildup in BHJ solar cells.[11,12,14,17]

In BHJ solar cells, free charge carriers are primarily transported to their respective contacts via drift in the built-in electric field. Charge carriers generated in the region of the active layer with no field must diffuse out of the no-field region in order to drift to the device contacts. Because charge-carrier

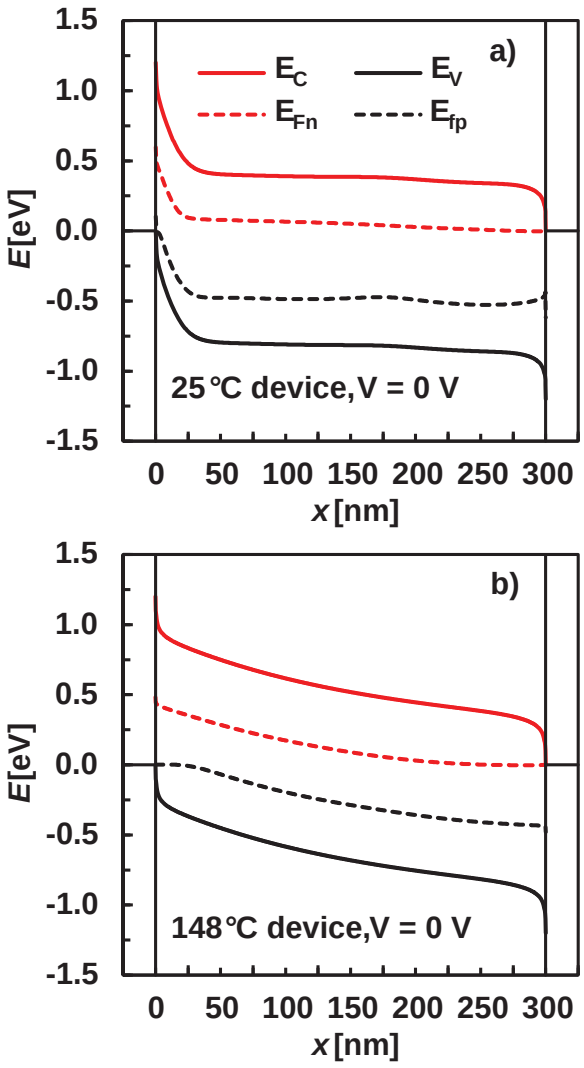

Figure 4. Simulated band diagram for a) 25 °C and b) 148 °C P3HT:PCBM solar cells at short-circuit conditions. Note that $x = 0$ nm and $x = 300$ nm correspond to the PEDOT:PSS—active layer interface and aluminum, and active layer interface, respectively. E_C: conduction band, E_V: valance band, E_{Fn}: electron quasi Fermi level, E_{Fp}: hole quasi Fermi level.

transport via diffusion is significantly slower than transport via drift, recombination in the no-field region is high and this region of the active layer does not significantly contribute to the device photocurrent. Thus, the buildup of holes in the active layer and screening of the built-in electric field in the device decreases the J_{SC} and FF of the 25 °C solar cell.

We quantitatively determined what fraction of the active layer is under a significant electric field as a function of anneal temperature in simulated 300 nm thick P3HT:PCBM solar cells (**Figure 5**). For consistency, we defined the electric field region as the portion of the active layer that has an electric field >10 kV cm^{-1} (more details are shown in Figure S3 in the Supporting Information). In these simulated devices, the width of the electric field region increases linearly with anneal temperature. Only the 148 °C device has a significant electric field extended throughout the whole 300 nm thick active layer. From these results, we conclude that a high FF can only be attained if

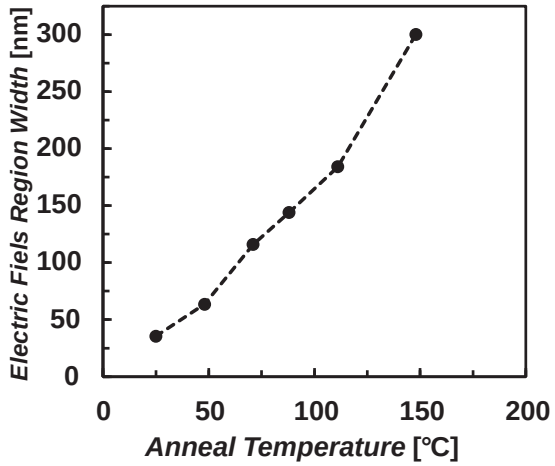

Figure 5. Width of the region of the active layer that is under a significant electric field as a function of anneal temperature for simulated thermally annealed 300 nm thick P3HT:PCBM solar cells.

a significant electric field extends throughout the whole device active layer. If the width of the electric field region is smaller than the active layer thickness, the region of the active layer with little or no electric field acts as a recombination zone and hinders charge extraction. Other researchers have also concluded that recombination zones with no electric field can degrade the performance of optically thick BHJ solar cells, but in these studies the cause of the electric field screening was attributed to inadvertent doping in the active layer rather than space-charge buildup.[16,53]

2.4. Mobility Required for FF >0.8

In this section, we simulate devices with $\mu_e = \mu_h$ in order to determine what charge-carrier mobility is needed to achieve a high FF in a device with balanced charge-carrier mobility. Space charge can build up in BHJ devices with $\mu_e = \mu_h$ for two primary reasons. First, due to the low mobility of intrinsic organic semiconductors, very large charge-carrier densities are needed to drive a given drift current in a BHJ solar cell. Thus, a large number of charge carriers reside in the active layer at steady state when the device is producing power. The presence of these charge carriers can cause space charge buildup and limit the FF of low mobility solar cells.[26] The second cause of space-charge buildup in these devices is the nonuniform charge-carrier generation profile in the active layer. Due to optical interference effects, the generation profile has maxima and minima throughout the active layer.[54] Even in semitransparent devices, which have fewer interference effects, the generation profile in the active layer is nonuniform. As a result of the nonuniform generation profile in BHJ solar cells, the distance that electrons and holes need to travel in order to reach their respective contacts is not equal. If one type of charge carrier needs to travel further through the active layer to reach its contact, that type of charge carrier can build up in the active layer and cause space-charge if the charge-carrier mobility is not high enough.

We find that $\mu_e = \mu_h > 9 \times 10^{-3}$ cm^2 V^{-1} s^{-1} is needed to achieve a 0.8 FF in a 300 nm thick P3HT:PCBM device (**Figure 6**).

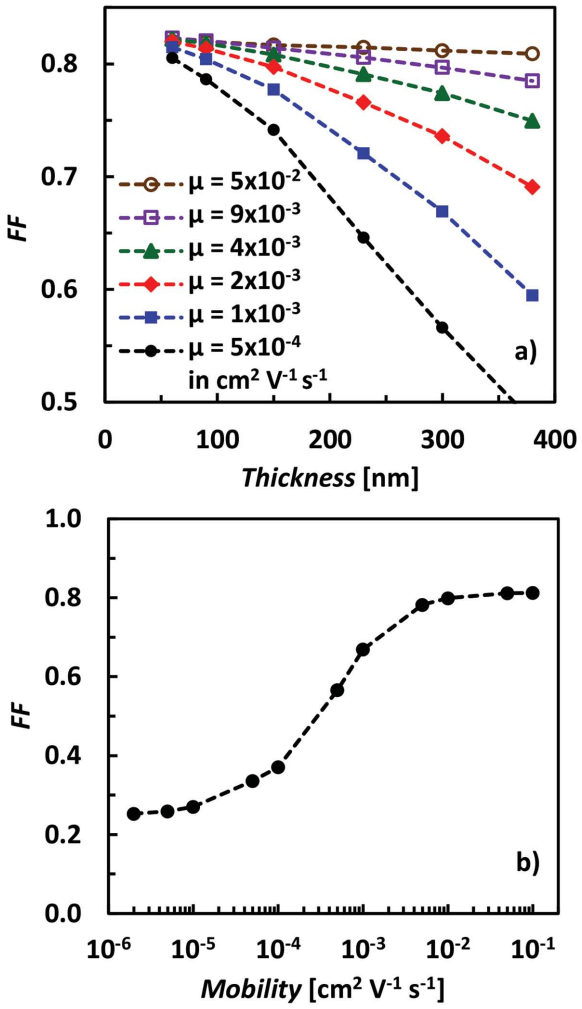

Figure 6. a) Fill factor as a function of active layer thickness for simulated P3HT:PCBM solar cells with $\mu_e = \mu_h$ and $k = 2 \times 10^{-12}$ cm^3 s^{-1}. b) Fill factor as a function of charge-carrier mobility for simulated 300 nm thick P3HT:PCBM solar cells with $\mu_e = \mu_h$ and $k = 2 \times 10^{-12}$ cm^3 s^{-1}.

Increasing the charge-carrier mobility to >10^{-2} cm^2 V^{-1} s^{-1} only leads to a modest improvement in FF because the FF begins to closely approach the maximum attainable FF for a 300 nm thick device with k and effective bandgap of P3HT:PCBM (Figure 6b). Decreasing the charge-carrier mobility, however, significantly reduces the FF of the 300 nm thick devices because the recombination rate is strongly affected by charge-carrier mobility in this intermediate mobility regime. For example, $\mu_e = \mu_h = 5\times10^{-4}$ cm^2 V^{-1} s^{-1} (similar to the hole mobility of annealed P3HT) yields an FF of only 0.57 in a 300 nm thick device and $\mu_e = \mu_h = 1 \times 10^{-3}$ and 5×10^{-3} cm^2 V^{-1} s^{-1} yield FFs of 0.67 and 0.78, respectively. These results qualitatively agree with those from drift-diffusion simulations of a small molecule-fullerene BHJ solar cell.[26] The electron mobility of our 148 °C P3HT:PCBM devices (5×10^{-3} cm^2 V^{-1} s^{-1}) is near the mobility required for a 0.8 FF in a thick device, but the hole mobility in these devices needs to be increased by a factor of 25 to match the required mobility. Taken together, these results show that relatively high charge-carrier mobility is needed to prevent space-charge buildup and minimize the rate of recombination in optically thick BHJ devices, even when the electron and hole mobility are balanced. We note that balanced electron and hole mobility are not necessary to achieve a high FF, and a device with imbalanced mobilities can still have a high FF if both μ_h and μ_e are high enough.

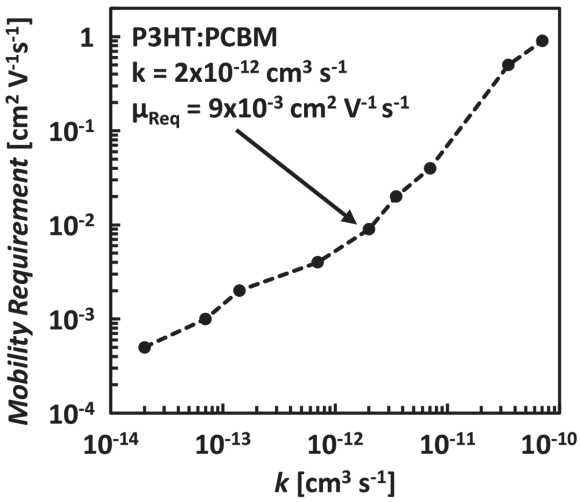

Figure 7. Charge-carrier mobility ($\mu_e = \mu_h$) required to achieve a 0.8 fill factor in a 300 nm thick simulated P3HT:PCBM solar cell as a function of recombination rate constant, k.

Not all polymer:fullerene BHJ systems have the same recombination rate constant, so we also examined how k affects the mobility required for a 0.8 FF in a 300 nm thick device. We simulated devices with a wide range of k and find that the mobility requirement is directly proportional to k (**Figure 7** and Table S1, Supporting Information). Thus, reducing k is an effective means of improving the FF of optically thick BHJ solar cells. In order for a device with mobility similar to the hole mobility of P3HT (5×10^{-4} cm^2 V^{-1} s^{-1}) to achieve a 0.8 FF with a 300 nm thick active layer, k needs to be reduced to 2×10^{-14} cm^3 s^{-1}. The range of experimentally measured values of k for BHJ solar cells is approximately 10^{-13} to 10^{-10} cm^3 s^{-1} (**Table 2**), so a k of 10^{-14} cm^3 s^{-1} only represents an order of magnitude decrease.[31,42,55–59] Alternatively, if k is increased to 10^{-11} cm^3 s^{-1}, then mobilities >10^{-1} cm^2 V^{-1} s^{-1} are needed to achieve a 0.8 FF in a 300 nm thick active layer. This result highlights that a low recombination rate constant strongly facilitates achieving a high FF in BHJ solar cells.

3. Discussion

P3HT has achieved a hole mobility >10^{-2} cm^2 V^{-1} s^{-1} and several donor–acceptor copolymers have recently achieved hole mobility >1 cm^2 V^{-1} s^{-1} in organic field-effect transistors (OFETs).[65–69] These high OFET mobilities demonstrate that conjugated polymer backbones are capable of transporting holes with mobility high enough to achieve a 0.8 FF in optically thick BHJ solar cells. Morphological analysis of the donor–acceptor copolymers with high OFET mobility revealed that rigid polymer backbones and closely π-stacked polymer aggregates

Table 2. Measured values of the recombination rate constant, k, for BHJ solar cells.

Material	k [cm^3 s^{-1}]
P3HT:PCBM as-cast[31,42]	1×10^{-12}, 2×10^{-11}
P3HT:PCBM annealed[31,42,43,60]	1×10^{-13}, 8×10^{-13}, 2×10^{-12}, 1×10^{-12}
P3HS[a]:PCBM annealed[43]	2×10^{-12}
PTB7[b]:$PC_{70}BM$[60]	3×10^{-12}
PCPDTBT[c]:$PC_{70}BM$[59,61]	5.5×10^{-11}, 2×10^{-10}
F-PCPDTBT[d]:$PC_{70}BM$[59]	1.5×10^{-11}
Si-PCPDTBT[e]:$PC_{70}BM$[43,57,61]	8×10^{-12}, 2×10^{-11}, 5×10^{-12}
KP115:PCBM[57,62]	3×10^{-12}, 2×10^{-12}
MDMO-PPV[f]:PCBM[63]	4×10^{-11}
Mono-DPP[g]:PCBM[58]	5×10^{-11}
Bis-DPP[h]:PCBM[58]	3×10^{-11}
P3HT:P(NDI2OD-T2)[i][64]	5×10^{-12}

[a]P3HS: poly(3-hexylselenophene); [b]PTB7: thieno[3,4 b]thiophene-alt-benzodithiophene; [c]PCPDTBT: poly[2,6-(4,4-bis(2-ethylhexyl)-4H-cyclopenta[2,1-b;3,4-b′]dithiophene)-alt-4,7-(2,1,3-benzothiadiazole)]; [d]F-PCPDTBT: poly[2,6-(4,4-bis(2-ethylhexyl)-4H-cyclopenta[2,1-b;3,4-b′]dithiophene)-alt-4,7-(5-fluoro-2,1,3-benzothiadiazole)]; [e]Si-PCPDTBT: poly[2,6-(4,4-bis(2-ethylhexyl)dithieno[3,2-b:2,3-d]silole)-alt-4,7-(2,1,3 benzothiadiazole)]; [f]MDMO-PPV: poly[2-methoxy-5-(3′,7′-dimethyloctyloxy)-1,4-phenylenevinylene]; [g]mono-DPP: 2,5-di-(2-ethylhexyl)-3,6-bis-(5″-n-hexyl-[2,2′,5,2″]terthiophen-5-yl)-pyrrolo[3,4-c]pyrrole-1,4-dione); [h]bis-DPP: 4,7-bis{2-[2,5-bis(2-ethylhexyl)-3-(5-hexyl-2,2′:5′,2″-terthiophene-5″-yl)-pyrrolo[3,4-c]pyrrolo-1,4-dione-6-yl]-thiophene-5-yl}-2,1,3-benzothiadiazole; [i] P(NDI2OD-T2): poly([N,N′-bis(2-octyldodecyl)-11-naphthalene-1,4,5,8-bis(dicarboximide)-2,6-diyl]-alt-5,5′-(2,2′-12-bithiophene)).

are crucial for achieving high hole mobility.[68,70] Rigid polymer backbones are important because intrachain charge-carrier transport occurs with very high mobility along planar, straight polymer chains.[69] If charge carriers encounter defects such as polymer chain ends or kinks/bends in the polymer chain, tightly π-stacked polymer aggregates facilitate fast interchain charge-carrier transport. Using these design rules, synthetic chemists may be able to synthesize new high mobility polymers for organic solar cells. The development of processing methods that align polymer chains perpendicular to the electrodes in a diode will also yield enhancements in hole mobility. The diode hole mobility of P3HT was increased by a factor of 20 (to 6×10^{-3} cm^2 V^{-1} s^{-1}) when P3HT chains were aligned vertically inside alumina pores.[71] This result shows that high mobility in a diode configuration is possible, but further research is needed to develop methods for polymer chain alignment in polymer–fullerene BHJs.

Researchers have experimentally measured k for several BHJ devices (Table 2), but little is known about what factors affect k and how one can design a BHJ with a low k. One strategy to reduce k for a given BHJ system is to spatially separate the electrons and holes in the device. One could attain this separation using energy cascades that make it energetically favorable for electrons and holes to reside in separate phases.[38,40] An example of a system with such an energy cascade is a BHJ made with a semicrystalline polymer. These BHJs have a three-phase morphology with pure PCBM and pure polymer phases and an amorphous phase consisting of polymer and fullerene mixed at the molecular level.[11,72,73] Because the bandgap of the polymer and fullerene is largest in the amorphous, mixed phase, the energy levels of the three phases are such that it is energetically favorable for the electrons and holes to reside in the pure PCBM and polymer phases.[50,74] Using the pure phases as spatially separated reservoirs for charge carriers effectively reduces the number of electrons and holes that drift through the amorphous, mixed phase when a given current is generated by the device at steady state. Thus, one could potentially reduce k by increasing the energetic offset between the amorphous, mixed phase, and the pure phases, which would decrease the number of charge carriers that reside in the mixed phase when the device is producing power.

At any given point in time when a BHJ solar cell is under illumination, a fraction of the photoexcited electrons and holes in the active layer are in charge-transfer states (CT-states). In an efficient solar cell where the CT states have a probability of separating that is close to one, the rate at which electrons and holes encounter each other, and even the probability of them separating if they do encounter each other, does not have a large impact on the rate of recombination because the pairs form and reseparate enough times for equilibrium to be reached between free charge carriers and CT states.[38,39,75] In equilibrium, the fraction of charge carriers that are in CT states is determined solely by the free energy difference between free charge carriers and CT states, with no dependence on kinetic parameters such as how quickly the charge carriers meet.[75] For a one-phase BHJ with homogeneous morphology, the rate of recombination is simply the density of CT states divided by the CT-state lifetime, which is the lifetime of the CT state when dissociation is not a possibility. Calculating the rate of recombination in BHJs with multiple phases is more complex, however, because the charge-carrier density in each phase is determined by its respective energy levels. Furthermore, CT states are only formed in phases that contain both polymer and fullerene, so the volume fraction and composition of the molecularly mixed phase in a BHJ affect the density of CT states.

Regardless of the number of phases in a BHJ, strategies to lower k include decreasing the density of the CT states in the BHJ and slowing down CT-state recombination. To decrease the density of CT states in a BHJ, one can reduce the CT-state binding energy[76,77] or decrease the volume fraction of mixed phase in the solar cell. The CT-state binding energy could be reduced by increasing the dielectric constant of the BHJ materials,[78,79] increasing the degree of CT-state delocalization,[76] and/or changing the distance between the polymer and fullerene at the molecular interface.[80] Processing BHJs to increase the polymer and fullerene degree of crystallization or aggregation or designing new molecules that easily form well-ordered morphologies may increase the degree of CT-state delocalization.[76] Furthermore, one can alter the distance between the polymer and fullerene by modifying the solubilizing side chains attached to the polymer.[81,82]

To slow down CT-state recombination, researchers should aim to increase the CT-state lifetime.[38] The CT-state lifetime may be affected by the electronic coupling between the polymer and fullerene at the CT-state heterojunction interface, which can in turn be affected by the polymer and fullerene orientation at the molecular interface and by the polymer and fullerene chemical structure.[82,83] To increase the lifetime of the CT state,

one could reduce the polymer–fullerene electronic coupling by either engineering how the polymer and fullerene pack next to each other to reduce wave function overlap or designing new polymers and fullerenes with specific wave functions that overlap poorly.[82,83] The CT-state energy and lifetime have proved difficult to probe in BHJ solar cells, but elucidating what factors affect these properties and determining how one can alter these properties through materials design will likely lead to significant improvements in BHJ solar cell performance.

4. Conclusion

Numerical device simulators are a powerful tool for investigating the recombination and charge-carrier transport properties of BHJ solar cells. With a device simulator, one can rapidly examine how variables such as charge-carrier mobility, active layer thickness, and the recombination rate constant affect device performance. We find that space-charge buildup and recombination significantly limit the performance of BHJ devices even when the electron and hole mobility are balanced. To minimize bimolecular recombination and space-charge buildup and achieve high FF in optically thick devices, relatively high charge-carrier mobility ($\approx 10^{-2}$ cm^2 V^{-1} s^{-1}) is needed. Furthermore, the mobility required to achieve a high FF in an optically thick device has a strong dependence on the recombination rate constant, k.

In order to reach 90% EQE and 0.8 FF with BHJ solar cells, future research should focus on increasing the active layer charge-carrier mobility and reducing k. The design rules for high-mobility OFET materials may provide insights for the synthesis of next-generation photovoltaic materials with exceptional hole mobility. Further research is also needed to elucidate what factors affect k and to determine how one can tailor the polymer–fullerene heterojunction to best reduce recombination. Researchers should also aim to increase the absorption coefficient of the organic semiconductors used in these BHJ solar cells because a 90% EQE could be achieved with a thinner active layer if the materials absorb light more strongly. Novel light-trapping schemes may also facilitate improvements in EQE, but effective light trapping in tandem solar cells is very challenging. Taken together, these findings show that 15% PCE could be achieved by simultaneously increasing the polymer and fullerene charge-carrier mobility to $\approx 10^{-2}$ cm^2 V^{-1} s^{-1} and decreasing the BHJ recombination rate constant to $<10^{-13}$ cm^3 s^{-1}.

5. Experimental Section

Device Fabrication: Indium tin oxide (ITO)-patterned glass substrates (Xin Yan Technologies LTD, 15 Ω $^{-1}$) were scrubbed with a dilute Extran 300 detergent and then ultrasonicated in dilute Extran 300 detergent for 15 min. The substrates were rinsed in deionized (DI) water for 5 min, ultrasonicated in acetone and isopropyl alcohol for 15 min each, and then rinsed in deionized water for 5 min. Substrates were placed in a ≈115 °C oven for 30 min and then exposed to a UV-ozone plasma for 15 min. Afterward, an aqueous solution of PEDOT:PSS (Clevios P VP AI 4083) was spin cast onto the substrates at 4000 rpm, and then the substrates were thermally annealed at 140 °C for 10 min. The substrates were transferred to a dry N_2 glovebox, with <5 ppm of O_2. Solutions were prepared in the glovebox by dissolving a 1:1 wt. ratio of P3HT (BASF P-200, 22 kDa molecular weight) and $PC_{60}BM$ (Nano-C, Batch BJ120703) in chloroform (Sigma-Aldrich, 99% purity). The solutions were dissolved overnight on a 30 °C hotplate before spin-casting. Solutions ranged from 10 mg total solids mL^{-1} to 30 mg total solids mL^{-1} to produce film thicknesses between 60 and 350 nm and were spin cast at 800 rpm for 45 s, with a ramp speed of 500 rpm s^{-1}. All thermal annealing was performed for 10 min and took place prior to metal electrode deposition. The metal electrodes consisted of 7 nm of calcium (Plasmaterials, 99.5% purity) and 250 nm of aluminum (Kurt J. Lesker, 99.999% purity) and were thermally evaporated at $\approx 10^{-6}$ Torr with a shadow mask that defined the active area of the devices to 0.1 cm^2. Preparation of the hole-only diodes was identical to that of the solar cells up to the metal electrode deposition. Instead of calcium and aluminum, 100 nm of gold (Sunshine Minting, Inc., 99.99% purity) was evaporated as the top contact and electron blocking layer.

Device Characterization: J–V measurements were conducted in a dry N_2 glovebox using a Keithley 2400 source meter and a Spectra-Physics 91160-1000 solar simulator, which was calibrated to one sun AM1.5 G using a NREL certified KG-5 filtered silicon photodiode. EQE and absorption measurements were performed with a Stanford Research Systems model SR830 DSP lock-in amplifier, and in the case of absorption, with an integrating sphere. For the IQE measurements, the active layer absorption was calculated by subtracting parasitic electrode absorption, calculated by transfer matrix modeling, from the total device absorption. Device active layer thicknesses were characterized using a Veeco Dektak profilometer. Hole mobility was calculated by taking the *J–V* measurements in the dark with a Keithley 2400 source meter. The hole mobility was extracted by fitting the SCLC regime to Equation (2) where J is the current density, V is the voltage, V_{bi} is the difference in work functions between the two contacts, L is the film thickness, and ε and μ_h are the material's dielectric constant and hole mobility, respectively. It was assumed that ε was 3 for P3HT and $V_{bi} = -0.1$ V was used. Devices of multiple thicknesses were tested to ensure the L^3 dependence properly described the experimental data.

$$J = \frac{9}{8}\varepsilon\varepsilon_0\mu_h\frac{(V - V_{bi})^2}{L^3} \quad (2)$$

Numerical Device Simulator: The P3HT:PCBM active layer was assumed to be a single-phase semiconductor with highest cccupied molecular orbital (HOMO) of 4.9 eV and lowest unoccupied molecular orbital (LUMO) of 3.7 eV. The contacts were assumed to be ohmic with work functions matched to the P3HT:PCBM HOMO and LUMO. The P3HT:PCBM effective density of states, N_0, and dielectric constant were set to 10^{22} cm^{-3} and 3.5, respectively, and it was assumed that the electron and hole mobility values were constant (no electric field dependence). A temperature of 298 K was assumed for all simulations and the AM1.5 spectrum was used to calculate the device generation profile.

Because our simulations assumed the P3HT:PCBM active layer was a single phase, our device model did not include excitons or charge-transfer states. It was assumed that only 80% of absorbed photons were converted to free charge carriers because the IQE of our optimized experimental P3HT:PCBM devices was approximately 74% (Figure S4, Supporting Information) and the IQE of P3HT:PCBM solar cells was shown to only reach ≈80% when the devices were placed under strong reverse bias.[84] Thus, ≈20% of the absorbed photons in the experimental P3HT:PCBM devices did not contribute to the photocurrent, regardless of the applied bias. This loss was attributed to inefficiencies in exciton harvesting and dead ends in the BHJ that trap charge carriers; some excitons generated in the BHJ were unable to diffuse to a heterojunction interface before recombining[85] and some charge carriers likely recombined quickly after becoming stuck in morphological traps.[11] The efficiency of photon to charge-carrier conversion will not be 80% for all BHJ systems and should be set to the value of the IQE obtained in reverse bias for a given device.

It was determined that the series resistance of the experimental P3HT:PCBM devices was directly proportional to the device active layer thickness and the device series conductivity was directly proportional to the P3HT hole mobility (Figure S5, Supporting Information). To incorporate series resistance with these properties into the simulation, the resistivity of the PEDOT:PSS contact in our device stack was varied. We first determined the PEDOT:PSS resistivity needed to reproduce the series resistance of a 205 nm thick 25 °C anneal device with hole mobility of 1.6×10^{-7} cm^2 V^{-1} s^{-1} by altering the PEDOT:PSS resistivity iteratively until a best fit between the experimental and simulated *J–V* curve was found. The best fit for the 205 nm thick 25 °C device was obtained with a PEDOT:PSS resistivity 1.1×10^6 Ω cm. The PEDOT:PSS resistivity for other simulated devices was determined using Equation (3) where ρ' is the PEDOT:PSS resistivity used to model a given device and μ', and L' are the P3HT hole mobility and active layer thickness, respectively, of that device. The individual *J–V* curve fits for ≈230 nm thick devices annealed at differing temperatures are shown in Figure S6 (Supporting Information).

$$\rho' = (1.1 \times 10^6\,\Omega\,\text{cm}) \times \frac{1.6 \times 10^{-7}\,\text{cm}^2\,\text{V}^{-1}\text{s}^{-1}}{\mu'} \times \frac{L'}{230\,\text{nm}} \quad (3)$$

When simulating PBDTTPD:PCBM BHJ solar cells of differing thickness, all parameters were kept constant except the active layer thickness. $\mu_h = 2.9 \times 10^{-5}$ cm^2 V^{-1} s^{-1} and $\mu_e = 1 \times 10^{-4}$ cm^2 V^{-1} s^{-1} for the active layer transport properties were used. The hole mobility was measured experimentally[11] and the electron mobility was assumed to be approximately equal to that in as-cast P3HT:PCBM BHJs[30] because PBDTTPD solar cells optimized without thermal annealing. The PBDTTPD HOMO was set to 5.2 eV and the PCBM LUMO was set to 3.7 eV. The best fit value of k (2.2×10^{-13} cm^3 s^{-1}) was determined iteratively and the PEDOT:PSS resistivity was set to 1×10^5 Ω cm for all simulations to account for series resistance. The strength of the active layer absorption coefficient was also adjusted to achieve the best agreement between the experimental and simulated device current. The individual *J–V* curve fits are shown in Figure S7 (Supporting Information).

Supporting Information

Supporting Information is available from the Wiley Online Library or from the author.

Acknowledgements

This work was supported by the Department of the Navy, Office of Naval Research Award No. N00014-14-1-0580. J.A.B. acknowledges government support by the Department of Defense (DoD) through the National Defense Science and Engineering Graduate Fellowship (NDSEG) Program. T.M.B. and S.M.S. acknowledge support from the National Science Foundation through the National Science Foundation Graduate Research Fellowship under Grant No. DGE-1147470 and acknowledge support from Stanford University through a Benchmark Stanford Graduate Fellowship. D.L. acknowledges support from Stanford University through an Undergraduate Advising and Research Major Grant.

Received: March 20, 2015
Revised: May 5, 2015
Published online: June 5, 2015

[1] Z. He, C. Zhong, S. Su, M. Xu, H. Wu, Y. Cao, *Nat. Photonics* **2012**, *6*, 591.
[2] S.-H. Liao, H.-J. Jhuo, Y.-S. Cheng, S.-A. Chen, *Adv. Mater.* **2013**, *25*, 4766.
[3] Y. Liu, J. Zhao, Z. Li, C. Mu, W. Ma, H. Hu, K. Jiang, H. Lin, H. Ade, H. Yan, *Nat. Commun.* **2014**, *5*, 5293.
[4] Z. A. Page, Y. Liu, V. V. Duzhko, P. Thomas, T. Emrick, T. P. Russell, T. Emrick, *Science* **2014**, *346*, 441.
[5] Q. Zhang, B. Kan, F. Liu, G. Long, X. Wan, X. Chen, Y. Zuo, W. Ni, H. Zhang, M. Li, Z. Hu, F. Huang, Y. Cao, Z. Liang, M. Zhang, T. P. Russell, Y. Chen, *Nat. Photonics* **2014**, *9*, 35.
[6] T. L. Nguyen, H. Choi, S.-J. Ko, M. A. Uddin, B. Walker, S. Yum, J.-E. Jeong, M. H. Yun, T. J. Shin, S. Hwang, J. Y. Kim, H. Y. Woo, *Energy Environ. Sci.* **2014**, *7*, 3040.
[7] X. Guo, N. Zhou, S. J. Lou, J. Smith, D. B. Tice, J. W. Hennek, R. P. Ortiz, J. T. L. Navarrete, S. Li, J. Strzalka, L. X. Chen, R. P. H. Chang, A. Facchetti, T. J. Marks, *Nat. Photonics* **2013**, *7*, 825.
[8] M. A. Green, K. Emery, D. L. King, S. Igari, W. Warta, *Prog. Photovoltaics Res. Appl.* **2015**, *23*, 1.
[9] S. Cho, N. E. Coates, J. S. Moon, S. H. Park, A. Roy, S. Beaupré, D. Moses, M. Leclerc, K. Lee, A. J. Heeger, *Nat. Photonics* **2009**, *3*, 297.
[10] Y. Liang, Z. Xu, J. Xia, S.-T. Tsai, Y. Wu, G. Li, C. Ray, L. Yu, *Adv. Mater.* **2010**, *22*, E135.
[11] J. A. Bartelt, Z. M. Beiley, E. T. Hoke, W. R. Mateker, J. D. Douglas, B. A. Collins, J. R. Tumbleston, K. R. Graham, A. Amassian, H. Ade, J. M. J. Fréchet, M. F. Toney, M. D. McGehee, *Adv. Energy Mater.* **2013**, *3*, 364.
[12] Z. M. Beiley, E. T. Hoke, R. Noriega, J. Dacuña, G. F. Burkhard, J. A. Bartelt, A. Salleo, M. F. Toney, M. D. McGehee, *Adv. Energy Mater.* **2011**, *1*, 954.
[13] S. Foster, F. Deledalle, A. Mitani, T. Kimura, K.-B. Kim, T. Okachi, T. Kirchartz, J. Oguma, K. Miyake, J. R. Durrant, S. Doi, J. Nelson, *Adv. Energy Mater.* **2014**, *4*, 1400311.
[14] V. D. Mihailetchi, J. Wildeman, P. W. M. Blom, *Phys. Rev. Lett.* **2005**, *94*, 126602.
[15] M. Lenes, L. J. A. Koster, V. D. Mihailetchi, P. W. M. Blom, *Appl. Phys. Lett.* **2006**, *88*, 243502.
[16] T. Kirchartz, T. Agostinelli, M. Campoy-Quiles, W. Gong, J. Nelson, *J. Phys. Chem. Lett.* **2012**, *3*, 3470.
[17] C. E. Small, S.-W. Tsang, S. Chen, S. Baek, C. M. Amb, J. Subbiah, J. R. Reynolds, F. So, *Adv. Energy Mater.* **2013**, *3*, 909.
[18] W. Li, S. Albrecht, L. Yang, S. Roland, J. R. Tumbleston, T. McAfee, L. Yan, M. A. Kelly, H. Ade, D. Neher, W. You, *J. Am. Chem. Soc.* **2014**, *136*, 15566.
[19] C. M. Proctor, J. A. Love, T.-Q. Nguyen, *Adv. Mater.* **2014**, *26*, 5957.
[20] D. A. Clugston, P. A. Basore, in *26th IEEE Photovolt. Spec. Conf. Anaheim* **1997**.
[21] M. Burgelman, P. Nollet, S. Degrave, *Thin Solid Films* **2000**, *361*, 527.
[22] Y. Liu, Y. Sun, A. Rockett, *Sol. Energy Mater. Sol. Cells* **2012**, *98*, 124.
[23] L. Koster, E. Smits, V. Mihailetchi, P. Blom, *Phys. Rev. B: Condens. Matter* **2005**, *72*, 085205.
[24] R. Häusermann, E. Knapp, M. Moos, N. A. Reinke, T. Flatz, B. Ruhstaller, *J. Appl. Phys.* **2009**, *106*, 104507.
[25] T. Kirchartz, B. E. Pieters, J. Kirkpatrick, U. Rau, J. Nelson, *Phys. Rev. B: Condens. Matter* **2011**, *83*, 115209.
[26] W. Tress, K. Leo, M. Riede, *Phys. Rev. B: Condens. Matter* **2012**, *85*, 155201.
[27] B. A. Collins, J. R. Tumbleston, H. Ade, *J. Phys. Chem. Lett.* **2011**, *2*, 3135.
[28] J. A. Bartelt, J. D. Douglas, W. R. Mateker, A. El Labban, C. J. Tassone, M. F. Toney, J. M. J. Fréchet, P. M. Beaujuge, M. D. McGehee, *Adv. Energy Mater.* **2014**, *4*, 1301733.
[29] C. J. Brabec, M. Heeney, I. McCulloch, J. Nelson, *Chem. Soc. Rev.* **2011**, *40*, 1185.
[30] V. D. Mihailetchi, H. X. Xie, B. de Boer, L. J. A. Koster, P. W. M. Blom, *Adv. Funct. Mater.* **2006**, *16*, 699.

[31] J. Kniepert, I. Lange, N. J. Van Der Kaap, L. J. A. Koster, D. Neher, *Adv. Energy Mater.* **2014**, *4*, 1301401.
[32] J. Kniepert, M. Schubert, J. C. Blakesley, D. Neher, *J. Phys. Chem. Lett.* **2011**, *2*, 700.
[33] C. M. Proctor, S. Albrecht, M. Kuik, D. Neher, T. Q. Nguyen, *Adv. Energy Mater.* **2014**, *4*, 1400230.
[34] A. Foertig, J. Kniepert, M. Gluecker, T. Brenner, V. Dyakonov, D. Neher, C. Deibel, *Adv. Funct. Mater.* **2014**, *24*, 1306.
[35] P. Langevin, *Ann. Chim. Phys.* **1903**, *28*, 433.
[36] K. Vandewal, S. Albrecht, E. T. Hoke, K. R. Graham, J. Widmer, J. D. Douglas, M. Schubert, W. R. Mateker, J. T. Bloking, G. F. Burkhard, A. Sellinger, J. M. J. Fréchet, A. Amassian, M. K. Riede, M. D. McGehee, D. Neher, A. Salleo, *Nat. Mater.* **2014**, *13*, 63.
[37] S. Albrecht, K. Vandewal, J. R. Tumbleston, F. S. U. Fischer, J. D. Douglas, J. M. J. Fréchet, S. Ludwigs, H. Ade, A. Salleo, D. Neher, *Adv. Mater.* **2014**, *26*, 2533.
[38] T. M. Burke, M. D. McGehee, *Adv. Mater.* **2014**, *26*, 1923.
[39] I. A. Howard, F. Etzold, F. Laquai, M. Kemerink, *Adv. Energy Mater.* **2014**, *4*, 1301743.
[40] C. Groves, *Energy Environ. Sci.* **2013**, *6*, 1546.
[41] J. Seifter, Y. Sun, A. J. Heeger, *Adv. Mater.* **2014**, *26*, 2486.
[42] R. Hamilton, C. G. Shuttle, B. O'Regan, T. C. Hammant, J. Nelson, J. R. Durrant, *J. Phys. Chem. Lett.* **2010**, *1*, 1432.
[43] A. Maurano, R. Hamilton, C. G. Shuttle, A. M. Ballantyne, J. Nelson, B. O'Regan, W. Zhang, I. McCulloch, H. Azimi, M. Morana, C. J. Brabec, J. R. Durrant, *Adv. Mater.* **2010**, *22*, 4987.
[44] A. Melianas, V. Pranculis, A. Devižis, V. Gulbinas, O. Inganäs, M. Kemerink, *Adv. Funct. Mater.* **2014**, *24*, 4507.
[45] S. T. Turner, P. Pingel, R. Steyrleuthner, E. J. W. Crossland, S. Ludwigs, D. Neher, *Adv. Funct. Mater.* **2011**, *21*, 4640.
[46] E. Verploegen, R. Mondal, C. J. Bettinger, S. Sok, M. F. Toney, Z. Bao, *Adv. Funct. Mater.* **2010**, *20*, 3519.
[47] B. Watts, W. J. Belcher, L. Thomsen, H. Ade, P. C. Dastoor, *Macromolecules* **2009**, *42*, 8392.
[48] B. A. Collins, E. Gann, L. Guignard, X. He, C. R. McNeill, H. Ade, *J. Phys. Chem. Lett.* **2010**, *1*, 3160.
[49] K. Vandewal, J. Widmer, T. Heumueller, C. J. Brabec, M. D. McGehee, K. Leo, M. Riede, A. Salleo, *Adv. Mater.* **2014**, *26*, 3839.
[50] S. Sweetnam, K. R. Graham, G. O. Ngongang Ndjawa, T. Heumueller, J. A. Bartelt, T. M. Burke, W. You, A. Amassian, M. D. McGehee, *J. Am. Chem. Soc.* **2014**, *136*, 14078.
[51] K. Vandewal, A. Gadisa, W. D. Oosterbaan, S. Bertho, F. Banishoeib, I. Van Severen, L. Lutsen, T. J. Cleij, D. Vanderzande, J. V. Manca, *Adv. Funct. Mater.* **2008**, *18*, 2064.
[52] C. Cabanetos, A. El Labban, J. A. Bartelt, J. D. Douglas, W. R. Mateker, J. M. J. Fréchet, M. D. McGehee, P. M. Beaujuge, *J. Am. Chem. Soc.* **2013**, *135*, 4656.
[53] G. F. A. Dibb, M.-A. Muth, T. Kirchartz, S. Engmann, H. Hoppe, G. Gobsch, M. Thelakkat, N. Blouin, S. Tierney, M. Carrasco-Orozco, J. R. Durrant, J. Nelson, *Sci. Rep.* **2013**, *3*, 1.
[54] L. A. A. Pettersson, L. S. Roman, O. Inganäs, *J. Appl. Phys.* **1999**, *86*, 487.
[55] A. Pivrikas, G. Juška, A. Mozer, M. Scharber, K. Arlauskas, N. Sariciftci, H. Stubb, R. Österbacka, *Phys. Rev. Lett.* **2005**, *94*, 176806.
[56] D. H. K. Murthy, A. Melianas, Z. Tang, G. Juška, K. Arlauskas, F. Zhang, L. D. A. Siebbeles, O. Inganäs, T. J. Savenije, *Adv. Funct. Mater.* **2013**, *23*, 4262.
[57] T. M. Clarke, D. B. Rodovsky, A. A. Herzing, J. Peet, G. Dennler, D. DeLongchamp, C. Lungenschmied, A. J. Mozer, *Adv. Energy Mater.* **2011**, *1*, 1062.
[58] C. M. Proctor, C. Kim, D. Neher, T. Q. Nguyen, *Adv. Funct. Mater.* **2013**, *23*, 3584.
[59] S. Albrecht, S. Janietz, W. Schindler, J. Frisch, J. Kurpiers, J. Kniepert, S. Inal, P. Pingel, K. Fostiropoulos, N. Koch, D. Neher, *J. Am. Chem. Soc.* **2012**, *134*, 14932.
[60] D. Rauh, C. Deibel, V. Dyakonov, *Adv. Funct. Mater.* **2012**, *22*, 3371.
[61] M. C. Scharber, M. Koppe, J. Gao, F. Cordella, M. A. Loi, P. Denk, M. Morana, H. J. Egelhaaf, K. Forberich, G. Dennler, R. Gaudiana, D. Waller, Z. Zhu, X. Shi, C. J. Brabec, *Adv. Mater.* **2010**, *22*, 367.
[62] T. M. Clarke, J. Peet, P. Denk, G. Dennler, C. Lungenschmied, A. J. Mozer, *Energy Environ. Sci.* **2012**, *5*, 5241.
[63] A. J. Mozer, G. Dennler, N. S. Sariciftci, M. Westerling, A. Pivrikas, R. Asterbacka, G. Juka, *Phys. Rev. B: Condens. Matter* **2005**, *72*, 035217.
[64] S. Roland, M. Schubert, B. A. Collins, J. Kurpiers, Z. Chen, A. Facchetti, H. Ade, D. Neher, *J. Phys. Chem. Lett.* **2014**, *5*, 2815.
[65] R. J. Kline, M. D. McGehee, E. N. Kadnikova, J. Liu, J. M. J. Fréchet, *Adv. Mater.* **2003**, *15*, 1519.
[66] H. Bronstein, Z. Chen, R. S. Ashraf, W. Zhang, J. Du, J. R. Durrant, P. Shakya Tuladhar, K. Song, S. E. Watkins, Y. Geerts, M. M. Wienk, R. A. J. Janssen, T. Anthopoulos, H. Sirringhaus, M. Heeney, I. McCulloch, *J. Am. Chem. Soc.* **2011**, *133*, 3272.
[67] H. N. Tsao, D. M. Cho, I. Park, M. R. Hansen, A. Mavrinskiy, D. Y. Yoon, R. Graf, W. Pisula, H. W. Spiess, K. Müllen, *J. Am. Chem. Soc.* **2011**, *133*, 2605.
[68] X. Zhang, H. Bronstein, A. J. Kronemeijer, J. Smith, Y. Kim, R. J. Kline, L. J. Richter, T. D. Anthopoulos, H. Sirringhaus, K. Song, M. Heeney, W. Zhang, I. McCulloch, D. M. DeLongchamp, *Nat. Commun.* **2013**, *4*, 2238.
[69] C. Luo, A. K. K. Kyaw, L. A. Perez, S. Patel, M. Wang, B. Grimm, G. C. Bazan, E. J. Kramer, A. J. Heeger, *Nano Lett.* **2014**, *14*, 2764.
[70] R. Noriega, J. Rivnay, K. Vandewal, F. P. V. Koch, N. Stingelin, P. Smith, M. F. Toney, A. Salleo, *Nat. Mater.* **2013**, *12*, 1038.
[71] K. M. Coakley, B. S. Srinivasan, J. M. Ziebarth, C. Goh, Y. Liu, M. D. McGehee, *Adv. Funct. Mater.* **2005**, *15*, 1927.
[72] W. Yin, M. Dadmun, *ACS Nano* **2011**, *5*, 4756.
[73] F. C. Jamieson, E. B. Domingo, T. McCarthy-Ward, M. Heeney, N. Stingelin, J. R. Durrant, *Chem. Sci.* **2012**, *3*, 485.
[74] S. Shoaee, S. Subramaniyan, H. Xin, C. Keiderling, P. S. Tuladhar, F. Jamieson, S. A. Jenekhe, J. R. Durrant, *Adv. Funct. Mater.* **2013**, *23*, 3286.
[75] T. M. Burke, S. Sweetnam, K. Vandewal, M. D. Mcgehee, *Adv. Energy Mater.* **2015**, *5*, 1500123.
[76] B. Bernardo, D. Cheyns, B. Verreet, R. D. Schaller, B. P. Rand, N. C. Giebink, *Nat. Commun.* **2014**, *5*, 3245.
[77] S. Gélinas, A. Rao, A. Kumar, S. L. Smith, A. W. Chin, J. Clark, T. S. van der Poll, G. C. Bazan, R. H. Friend, *Science* **2014**, *343*, 512.
[78] L. J. A. Koster, S. E. Shaheen, J. C. Hummelen, *Adv. Energy Mater.* **2012**, *2*, 1246.
[79] S. Chen, S. W. Tsang, T. H. Lai, J. R. Reynolds, F. So, *Adv. Mater.* **2014**, *26*, 6125.
[80] E. H. Yonemoto, G. B. Saupe, R. H. Schmeh, S. M. Hubig, R. L. Riley, B. L. Iverson, T. E. Mallouk, *J. Am. Chem. Soc.* **1994**, *116*, 4786.
[81] T. W. Holcombe, J. E. Norton, J. Rivnay, C. H. Woo, L. Goris, C. Piliego, G. Griffini, A. Sellinger, J.-L. Brédas, A. Salleo, J. M. J. Fréchet, *J. Am. Chem. Soc.* **2011**, *133*, 12106.
[82] K. R. Graham, C. Cabanetos, J. P. Jahnke, M. N. Idso, A. El Labban, G. O. Ngongang Ndjawa, T. Heumueller, K. Vandewal, A. Salleo, B. F. Chmelka, A. Amassian, P. M. Beaujuge, M. D. McGehee, *J. Am. Chem. Soc.* **2014**, *136*, 9608.
[83] Y. Yi, V. Coropceanu, J. L. Brédas, *J. Am. Chem. Soc.* **2009**, *131*, 15777.
[84] G. F. Burkhard, E. T. Hoke, Z. M. Beiley, M. D. McGehee, *J. Phys. Chem. C* **2012**, *116*, 26674.
[85] G. F. Burkhard, E. T. Hoke, S. R. Scully, M. D. McGehee, *Nano Lett.* **2009**, *9*, 4037.